

MARINE DURABILITY OF 15-YEAR-OLD UNCRACKED AND PRECRACKED CONCRETE SPECIMENS MADE WITH DIFFERENT CEMENTS

(Reprinted from Proceedings of JSCE, No.697/V-54, February 2002)



T. U. MOHAMMED



Toru YAMAJI



Toshiyuki AOYAMA



Hidenori HAMADA

The marine durability of 15-year-old uncracked and precracked concrete specimens made with ordinary Portland (OPC), slag (types A (SCA), B (SCB) and C (SCC)), and fly ash (type B (FACB)) cements is investigated. Compressive strength, chloride ingress, corrosion of steel reinforcing bars, and crack healing are evaluated. The degree of chloride ingress and degree of steel bar corrosion are found to be ordered as OPC>FACB>SCA>SCB>SCC. Crack healing is observed for small crack widths (≤ 0.5 mm) irrespective of the cement type. Large crack widths, such as 1.5, 2 and 5 mm, do not heal and significant loss of diameter is observed. Voids at the steel-concrete interface lead to the formation of corrosion pits.

Keywords: *fly ash cement, marine durability, ordinary Portland cement, slag cement.*

Tarek Uddin Mohammed is a Research Engineer at Materials Division of Port and Airport Research Institute, Japan. He obtained his D. Eng. from Tokyo Institute of Technology (TIT), M. Eng. from Asian Institute of Technology (AIT), and B. Eng. from Bangladesh University of Engineering and Technology (BUET), Dhaka, Bangladesh. His research interest covers corrosion of steel bars in concrete, marine durability of concrete structures, interfaces in concrete, and ASR expansion of concrete. He is a member of JSCE.

Toru Yamaji is a Research Engineer at Materials Division of Port and Airport Research Institute, Japan. He obtained his M. Eng. and B. Eng. from Kyushu University. His research interest covers marine durability of concrete structures, utilization of stainless steel in concrete, and corrosion inhibitors. He is a member of JSCE.

Toshiyuki Aoyama is a Civil Engineer of PS Corporation, Japan. He obtained his M. Eng. and B. Eng. from Nagaoka University of Technology. His research interest covers durability of pre-stressed concrete structures, repair and maintenance of pre-stressed concrete structures. He is a member of JSCE.

Hidenori Hamada is the Chief of Materials Division of Port and Airport Research Institute, Japan. He received his D. Eng., M. Eng. and B. Eng. from Kyushu University. His research interests covers marine durability of concrete structures, utilization of optical fiber for health monitoring of concrete structures, repair and rehabilitation of marine concrete structures. He is a member of JSCE.

1. INTRODUCTION

Concretes are designed with blended cements so as to achieve better durability, reduce the problem of by-product disposal for the steel-making industry and thermal power plants, and also indirectly reduce emissions of carbon dioxide into the atmosphere. Numerous studies have been carried out to verify the performance of concretes made with blended cements [1~5]. However, studies on the long-term performance of such concretes are still necessary and will assist in improving their acceptability worldwide.

In this research, 15-year-old uncracked concrete specimens (cylinders of diameter 15 cm and height 30 cm) and precracked concrete specimens (prisms measuring 10x10x60 cm) made with ordinary Portland cement (OPC), slag cements of type A, B and C (SCA, SCB, and SCC), and fly ash cement of type B (FACB) are investigated after exposure in the tidal zone. These cements are as specified in the Japanese standards (JIS R5211-1992 and JIS R5213-1992). Investigations are carried out for concrete compressive strength, ultrasonic pulse velocity, water- and acid-soluble chloride-ion concentrations, and crack healing, as well as electrochemical and physical evaluations of steel reinforcing bar corrosion. The results are compared for the various cement types. Moreover, the study also looks at the harmful effects of the presence of voids at the steel-concrete interface. The findings of this study are a very useful aid to judging the marine durability of concretes made with different cements.

2. SCOPE AND FLOW OF INVESTIGATION

The investigation considered uncracked cylinder specimens of diameter 15 cm and height 30 cm and precracked prism specimens of size 10x10x60 cm. The specimens were made with ordinary Portland cement (OPC), slag cement of type A, B, and C (SCA, SCB, and SCC), and fly ash cement of type B (FACB). The water-to-cement ratio was 0.45 throughout. Based on these variables, five reinforced concrete specimens were investigated. The specimens were exposed in a tidal pool after 28 days of standard curing, and exposure continued until this investigation, i.e., for 15 years. A flow chart of the investigations is shown in Fig. 1. The cracked and uncracked specimens were investigated in parallel.

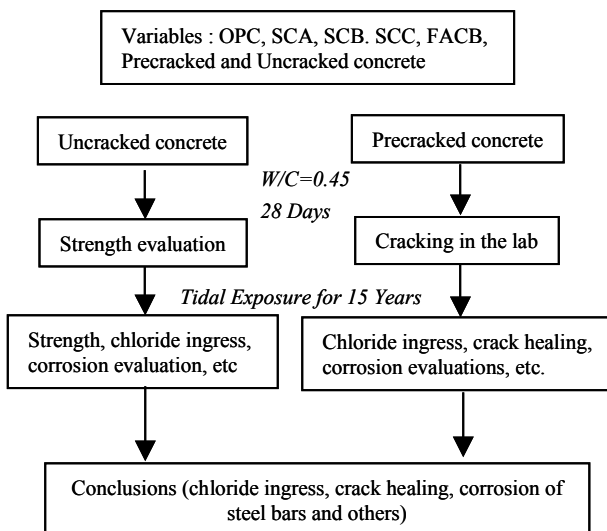


Fig. 1 Flow of investigation

Table 2 Aggregate properties

	Specific Gravity	Absorption (%)	Fineness Modulus
Sand	2.64	1.02	2.89
Gravel	2.76	1.10	6.66

Table 1 Physical and chemical composition of cement

	OPC	SCA	SCB	SCC	FACB
Specific Gravity	3.16	3.07	3.03	2.97	2.97
Blaine Fineness, cm ² /g	3190	3610	3700	3980	3190
Ignition Loss (%)	0.7	0.9	0.7	0.9	0.6
SiO ₂ (%)	21.3	24.9	26.5	28.9	20.4
Al ₂ O ₃ (%)	5.3	7.8	9.2	11.3	4.7
CaO (%)	64.4	56.8	53.4	47.9	54.2
MgO (%)	2.2	3.8	4.3	5.2	1.3
SO ₃ (%)	1.9	2	2	2	1.9
Na ₂ O (%)	0.28	-	-	-	0.45
K ₂ O (%)	0.6	-	-	-	0.51
TiO ₂ (%)	0.37	-	-	-	-
MnO (%)	0.1	-	-	-	-
Fe ₂ O ₃ (%)	2.6	2	1.8	1.1	2.9
P ₂ O ₅ (%)	0.3	-	-	-	-
C (%)	0.01	-	-	-	-
S (%)	0	-	-	-	-

- data not available

Table 3 Chemical composition of steel bar

C (%)	Si (%)	Mn (%)	P (%)	S (%)
0.1	0.21	0.66	0.02	0.02

3. EXPERIMENTAL PROCEDURE

(1) Materials

Ordinary Portland cement (OPC), slag cement of types A, B and C (SCA, SCB, and SCC), and fly ash cement of type B (FACB) was used for the investigations. These cements were as specified in reference [6]. Definitions of the blended cements and their specified physical and chemical compositions can be obtained in JIS R5211-1992 and JIS R5213-1992. The cement compositions are listed in **Table 1**. Crushed river gravel and sand were used as the coarse and fine aggregates, respectively. The specific gravity, absorption, and fineness modulus of these aggregates are listed in **Table 2**. Japanese Industrial Standard (JIS) steel bar (JIS SR 24) of diameter 9 mm was used. The yield strength of the steel bar was 230 MPa. The chemical composition of the steel bars is listed in **Table 3**.

(2) Mix Proportions

The concrete mix proportions are listed in **Table 4**. The water-to-cement ratio was 0.45 throughout. The slump of the fresh concrete was fixed at 8 ± 1 cm, and the air content at $4 \pm 1\%$. Both air-entraining and air-entraining water-reducing agents were used according to the cement weight. Mixing water was plain tap water.

Table 4 Mix proportions of concrete

	OPC	SCA	SCB	SCC	FACB
G_{max} (mm)	20	20	20	20	20
Slump (cm)	8 ± 1				
Air (%)	4 ± 1				
W/C (%)	45	45	45	45	45
s/a (%)	41	42	41	41	41
W (kg/m^3)	162	160	160	162	160
C (kg/m^3)	360	356	355	360	356
S (kg/m^3)	738	756	736	714	733
G (kg/m^3)	1110	1091	1108	1120	1103
AEWRA (kg/m^3)	3.60	3.56	3.55	3.60	3.56
AEA (mL/m^3)	360	356	355	360	356

The letters W, C, G, S (s), and a represent water, cement, gravel, sand and aggregate (coarse and fine), respectively. AEA and AEWRA mean air-entraining admixture, and air-entraining water-reducing admixture, respectively.

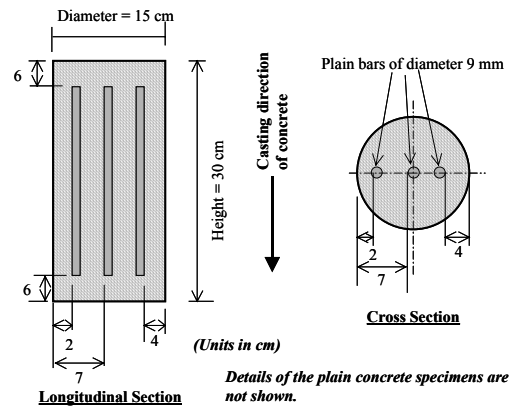


Fig. 2 Details of uncracked cylindrical specimens

Table 5 Specimen plans

Case	Uncracked Specimens (Cylinder)		Precracked Specimens (Prism)
	Plain	Reinforced*	
OPC	6+3	2	3
SCA	6+3	2	3
SCB	6+3	2	3
SCC	6+3	2	3
FACB	6+3	2	3

Six plain concrete specimens were tested at 28-days to determine compressive strength. *One specimen per case is retained for detailed analysis (porosity, SEM, XRD, and EPMA).

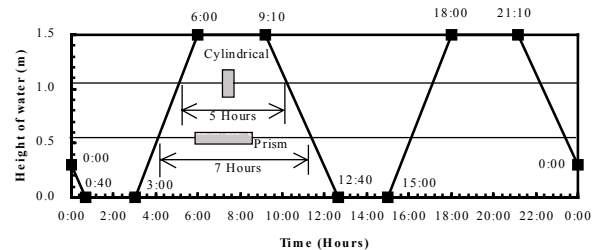


Fig. 3 Variation of water level in the tidal pool and the locations of the cylindrical and prism specimens

Table 6 Physical properties and chemical compositions of seawater

Sp. gr.	pH	Na ppm	K ppm	Ca ppm	Mg ppm	Cl ppm	SO ₄ ppm	CO ₃ ppm
1.02	7.77	9290	346	356	1167	17087	2378	110

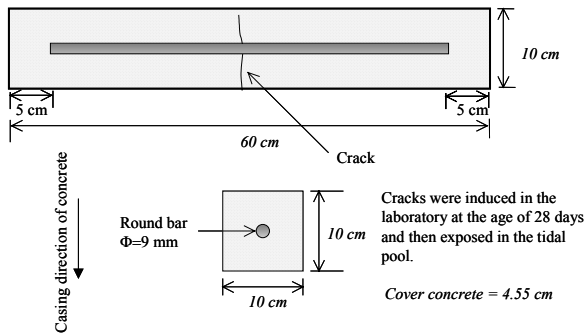


Fig. 4 Details of precracked prism specimens

Table 7 Applied load and crack widths at the tensile face of the prism specimens

Specimen	Applied Load (in tons) and Crack Width (mm) at the Tensile Face*		
	1	2	3
OPC	0.6 (0.2)	0.7 (0.1)	0.79 (0.1)
SCA	0.62 (0.1)	0.7 (0.3)	0.62 (0.25)
SCB	0.64 (0.5)	0.62 (0.2)	0.6 (4.0)
SCC	0.6 (1.9)	0.49 (0.15)	0.6 (2.7)
FACB	0.7 (0.1)	0.62 (0.2)	0.58 (1.5)

*The figures in brackets are crack widths in millimeter. Numbers 1, 2, and 3 are the specimen numbers for each case.

(3) Specimens and Exposure Conditions

The specimen plan was as shown in Table 5. The layout of the uncracked specimens is shown in Fig. 2. Plain and reinforced cylindrical specimens of diameter 15 cm and length 30 cm were fabricated. In each reinforced specimen, three round steel bars of diameter 9 mm and length 18 cm were embedded at cover depths of 2, 4, and 7 cm. After standard curing, the plain concrete specimens were tested for compressive strength evaluation at 28 days. The remaining specimens were exposed in the tidal pool till the age of 15 years. The locations of specimens in the tidal pool are shown in Fig. 3, along with the pool's water level variations. The specimens were placed at a level about 0.6 m below high water level. The average distance from high water level to the mid-height of a specimen was 0.45 m, and air-drying and submerged periods were about 7 and 5 hours, respectively. Seawater was automatically pumped into the pool directly from the sea and drained back out to the sea at regular intervals. The location of the pool was at an approximate latitude of 35° N and longitude of 138° E. The pool was free from freezing and thawing. The physical properties and chemical composition of the seawater are listed in Table 6.

The layout of the precracked prism specimens is shown in Fig. 4. The specimens size was 10x10x60 cm. In each specimen, a round steel bar of diameter 9 mm and length 50 cm was embedded with a cover of 4.55 cm; that is, at the specimen center. After 28 days of standard curing, cracks were induced in the specimens in the laboratory. The cracking loads and crack widths on the tensile surface were as listed in Table 7. After cracking, the specimens were exposed in the tidal pool at a point 0.9 m below the high water level. Air-drying and submerged periods for these specimens were again about 5 and 7 hours, respectively. Other details of the tidal pool are as already noted.

(4) Measurements and Evaluations

a) Before Exposure

The concrete's 28-day compressive strength was measured as per JIS A1108. In each case, six specimens were tested. The prism specimens were cracked by bending after 28 days of standard curing. Crack widths on the tensile surface of the specimens and the applied loads were, as already noted, as shown in Table 7.

b) After 15 Years of Exposure

After 15 years, the specimens were transferred from the exposure site to the laboratory and cleaned with seawater. The laboratory was furnished with a supply of fresh seawater direct from the sea. The compressive strength of plain concrete specimens was measured according to JIS A1108 after keeping the specimens in the laboratory for 24 hours under seawater. The ultrasonic pulse velocity through the center of the plain cylinder specimens was measured (with a pulse frequency of 54 kHz) prior to the compressive strength tests. No electrical wires were originally connected to the embedded steel bars, so to carry out electrochemical investigations on cylindrical specimens an 8 cm section was cut from the top. Wires were connected to the steel bars at different cover depths. The connecting points and their surroundings were sealed with epoxy resin. The half-cell potential was measured using a Ag/AgCl half-cell. Based on the half-cell potential, the probability of corrosion was evaluated as per ASTM C 876 [7]. The polarization resistance and concrete resistance were measured by an AC impedance technique. For these measurements, the low frequency was set at 20 mili-Hz and the maximum frequency at 10 Hz. Measurements were carried out while the specimens remained submerged in seawater surrounded with a stainless steel counter-electrode. Micro-cell corrosion current was estimated based on the polarization resistance data, with degree of corrosion classified as negligible, low, moderate, and high for estimated current densities of <0.1, 0.1-

0.5, 0.5-1 and $>1 \mu\text{A}/\text{cm}^2$, respectively [8]. After these measurements, the anodic polarization curves of the embedded steel bars were also measured. For these measurements, the potential of the steel bars was shifted from its natural value to 1 V positive with a scan rate of 1 mV/sec using a potentiostat. The passivity of the steel bars was evaluated (as 0, 1, 2, 3, 4, or 5) from the measured anodic polarization curves [9]. A higher passivity means less corrosion activity. As with the cylindrical specimens, a length of 6 cm was cut from one end of the prism specimens to facilitate the connection of electrical wires to the embedded steel bars. Polarization resistance, concrete resistance, and half-cell potential over the length of the steel bar of the prism specimens in the cracked region were measured with the same portable corrosion monitor. In this case, the measurements were carried out after keeping the specimens submerged in seawater for 24 hours. The corrosion sensor was furnished with a counter-electrode, a guard-electrode, and a Ag/AgCl half-cell. After electrochemical measurements, the specimens were broken open and the steel bars removed. The corroded area over the steel bars was measured, and then the steel bar were immersed in a 10% diammonium hydrogen citrate solution for 24 hours and cleaned with a steel wire brush. The diameter of the pits revealed in this process was measured using an optical microscope, while their depth was obtained using a needle marked with known depths. Pits measuring less than 0.5 mm in depth were not counted.

The carbonation depth of the specimens was evaluated after spraying 1% phenolphthalein solution on the freshly cut surface. Water- and acid-soluble chloride-ion concentrations of the cylinder specimens were measured for depth ranges 0.5-1.5, 1.5-2.5, 3.5-4.5, and 6.5-7.5 cm. This was done by cutting discs of thickness 8 cm from the center of reinforced concrete specimens. After cutting, the steel-concrete interface was checked with an optical microscope. A 2 cm-strip was then cut from the middle of the concrete disc and finally concrete samples were taken according to the depth ranges mentioned above. Before milling of these samples, the coarse aggregate particles were removed carefully. The water- and acid-soluble chloride-ion concentrations were measured as per JCI SC4. In the case of prism specimens, only the water-soluble chloride-ion concentration was measured surrounding the steel bars (< 5 mm from the steel bar) at cracked and uncracked regions. To measure the chloride-ion concentration in the cracked region, a strip of 5 cm was cut across the specimen such that the crack ran through the middle of the strip. This strip was again cut to remove the portion of concrete within 5 mm of the steel bar. Finally, concrete samples surrounding the steel bars were collected and the water-soluble chloride-ion concentration in the concrete was measured as before. As with the cracked region, the chloride-ion concentration in the uncracked region (10-15 cm from the end of the specimen) was also measured. Based on the water-soluble chloride ion concentration, the probability of corrosion was categorized as negligible, possible, probable, or certain, as listed in **Table 8** [10]. During the investigation, it was found that narrow cracks were healed gradually. On observing this, the chemical composition of deposits in the cracks was confirmed using an EPMA (Electron Probe Micro Analyzer). Moreover, the surface morphology of the deposits was also checked using an SEM (Scanning Electron Microscope).

Table 8 Chloride threshold values [10]

Chloride-ion Concentration (wt. % of cement)	Probability of Corrosion
< 0.4	Negligible
0.4 - 1.0	Possible
1.0 - 2.0	Probable
> 2.0	Certain

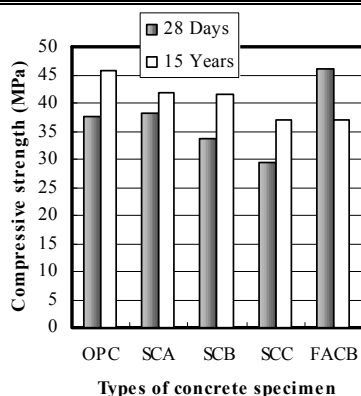


Fig. 5 Compressive strength of concrete (28 days and 15 years)

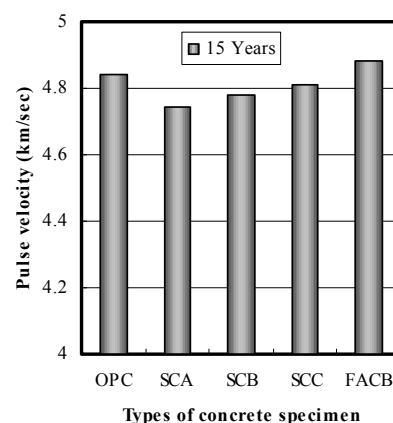


Fig. 6 Pulse velocity through the center of concrete specimens (at 15 years)

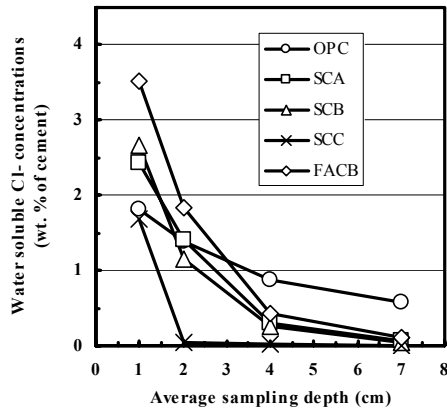


Fig. 7 Water soluble chloride-ion concentrations (Uncracked concrete)

Table 9 Possibilities of corrosion of steel bars

Cover (cm)	Probability of Corrosion (Based on Table 8)				
	OPC	SCA	SCB	SCC	FACB
2	Probable	Probable	Probable	Negligible	Probable
4	Possible	Negligible	Negligible	Negligible	Possible
7	Possible	Negligible	Negligible	Negligible	Negligible

4. EXPERIMENTAL RESULTS AND DISCUSSION

(1) Carbonation Depth

Carbonation depth was negligible in all specimens irrespective of cement type, and as a result it could not be compared among the cements investigated here. This clarifies that the specimens were subjected only to chloride-ion induced corrosion.

(2) Compressive Strength and Pulse Velocity

The concrete compressive strengths at the age of 28 days and after 15 years of exposure are compared in **Fig. 5**. Compared to the 28-day strength, OPC, SCA, SCB, and SCC were found to have gained in strength. Beyond 28 days, the continued hydration of concrete would lead to a strength gain. However, this gain could not be evaluated in this study as strength was measured only at 28 days and 15 years. However, it was clear that after 15 years of exposure the strength of concrete made with OPC, SCA, SCB, and SCC still satisfied the initial design strength. As compared to the strength at 28 days, a reduction (of about 20%) in strength is observed in the case of concrete made with FACB. Such a strength reduction can be expected because of the greater ettringite formation in the case of FACB. A further detailed investigation of specimen microstructure and mineralogy is planned so as to confirm this result. The strength development of concrete under continued exposure is also reported in some of the cited literature [11–13]. Among these findings, a study of OPC and SCB has shown that concrete strength increases till the age of 5 years and thereafter falls off gradually, and after 20 years of exposure, it reaches or falls below the 28-day strength [11]. This strength reduction was explained by ettringite formation based on mineralogical analysis of the specimens.

The ultrasonic pulse velocity through the center of concrete specimens made with different cements is shown in **Fig. 6**. The pulse velocity varied between 4.74 and 4.88 km/s. No significant variation in pulse velocity was observed among the cases investigated here. The initial pulse velocity in the concrete specimens was not measured, so changes in pulse velocity with compressive strength cannot be commented on here.

(3) Chloride-ion Ingress into Concrete

a) Uncracked Concrete (Cylinder Specimens)

Water-soluble chloride-ion profiles for the concretes are shown in **Fig. 7**. Relatively more chloride-ions penetrated to greater depth in concrete made with OPC as compared to SCA, SCB, SCC, and FACB. Where slag and fly ash cements were used, more chloride-ions were observed to accumulate in the surface region; however, their concentration quickly fell to a negligible value with depth. The same results have been observed in another study on 10-year-old concrete specimens [14]. The probability of steel bar corrosion was evaluated based on the chloride-ion concentrations as given in **Table 8**. The results of this evaluation are listed in **Table 9**. In the case of SCC, the probability of corrosion was found to be negligible irrespective of the cover depth. Based on these results, the degree of chloride ingress into uncracked concrete is determined to be ordered as OPC>FACB>SCA>SCB>SCC.

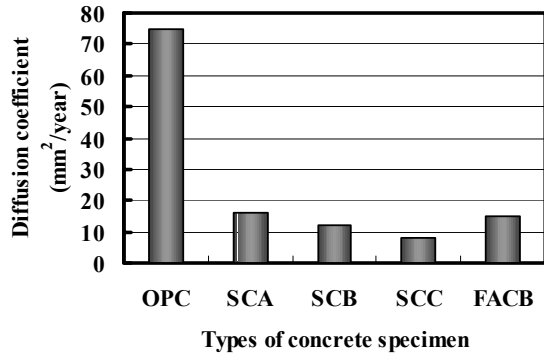


Fig. 8 Diffusion coefficient of chloride-ion in concrete

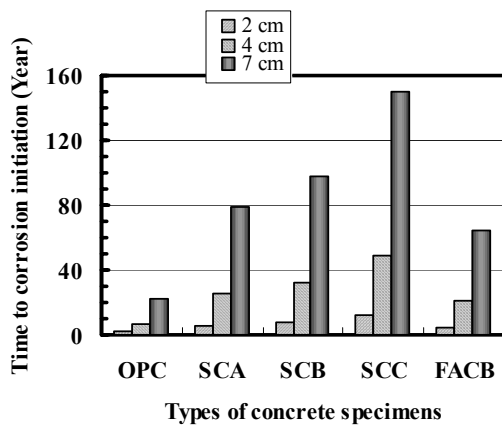


Fig. 9 Time to corrosion initiation for different cements

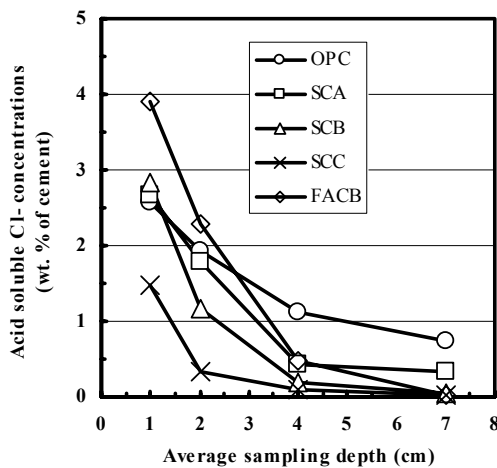


Fig. 10 Acid-soluble chloride-ion concentrations

Table 10 Ratio of acid- to water-soluble chloride-ion concentrations

*Depth (cm)	Ratio of Acid to Water Soluble Cl ⁻ Conc.				
	OPC	SCA	SCB	SCC	FACB
1	1.427	1.093	1.061	0.882	1.108
2	1.392	1.264	1.006	8.013	1.249
4	1.278	1.433	0.769	6.711	1.125
7	1.262	5.456	1.183	2.797	0.313

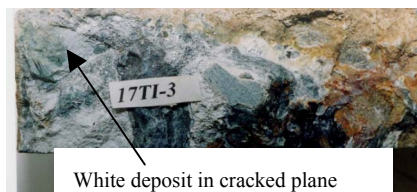
*Depth means the average sampling depth.

Table 11 Water-soluble chloride-ion concentration in cracked and uncracked regions of prism specimens

Specimen	Crack Width (mm) and Water-Soluble Chloride-ion Concentrations (wt. % of C) *		
	1	2	3
OPC	0.2 (1.28) ((1.27))	0.1 (1.14) ((0.64))	0.1 (1.38) ((1.41))
SCA	0.1 (0.33) ((0.17))	0.3 (0.78) ((0.23))	0.2 (0.49) ((0.43))
SCB	0.3 (0.45) ((0.31))	0.1 (0.41) ((0.28))	5 (3.2) ((0.16))
SCC	1.5 (1.67) ((0.19))	0.1 (0.37) ((0.23))	2 (1.84) ((0.69))
FACB	0.1 (0.9) ((0.67))	0.3 (0.82) ((0.29))	0.5 (1.42) ((0.27))

*The figures in (.) and ((.)) represent chloride-ion concentrations in cracked and uncracked regions, respectively. The figures without bracket indicates represent crack widths. Unhealed cracks are shown in bold-italic type.

White deposit on concrete surface and in the crack



White deposit in cracked plane

Photographs of concrete surface (top) and cracked plane (bottom) after splitting along the crack.

Fig. 11 Crack healing – FACB (Crack width = 0.5 mm)

An attempt was made to determine the diffusion coefficients of chloride ions in the concrete. Fick's Second Law of diffusion is commonly used to predict the diffusion of chloride ions in concrete. Its closed form solution is expressed as below in the literature [15].

$$C(x,t) = C_o \left(1 - \operatorname{erf} \left[\frac{x}{2\sqrt{D_{ac}t}} \right] \right)$$

Where, $C(x,t)$ is the chloride-ion concentration at depth x (mm) and time t (years), C_o is the chloride-ion concentration at the surface as a weight percentage of cement, and D_{ac} is the apparent diffusion coefficient in mm^2/year . Here, C_o was assumed to be equal to the chloride-ion concentration at a mean sampling depth of 1 cm. The estimated average diffusion coefficients for different cements are shown in **Fig. 8**. Based on these results, chloride diffusion in concrete is also found to be ordered as $\text{OPC} > \text{FACB} > \text{SCA} > \text{SCB} > \text{SCC}$. The time to corrosion initiation was defined as the time taken before the chloride-ion concentration reached 0.4% of the cement by weight surrounding the steel bars. The estimated times to corrosion initiation are shown in **Fig. 9** for design cover depths of 2, 4, and 7 cm. It can be clearly observed that slag cement, especially SCC, very effectively increases the time to corrosion initiation. If a concrete is made with SCC and the design cover is 7 cm, the theoretical time to initiation of steel bar corrosion is about 150 years.

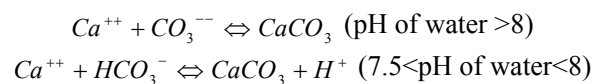
Acid-soluble chloride-ion profiles for concretes made with the different cements are shown in **Fig. 10**. From these results, the chloride ingress into the concrete is determined to be ordered as $\text{OPC} > \text{FACB} > \text{SCA} > \text{SCB} > \text{SCC}$. The ratios of acid- to water-soluble chloride-ion concentrations are calculated based on the data presented in **Figs. 7** and **10**, and these are listed in **Table 10**. This can be used to judge the chloride-binding ability of the cements. The ratio is higher for OPC compared to the other cements. This indicates that the chloride-binding ability of concrete made with OPC is the best compared to concretes made with fly ash and slag cements. It is supposed that this is due to the superior chloride complex-forming ability, which results in the formation of an insoluble calcium chloroaluminate compound that helps to reduce the amount of free chloride ions [16~18]. There are some contradictory data in **Table 10**, especially at higher depths, due to the very low chloride-ion concentrations.

b) Cracked Concrete (Prism Specimens)

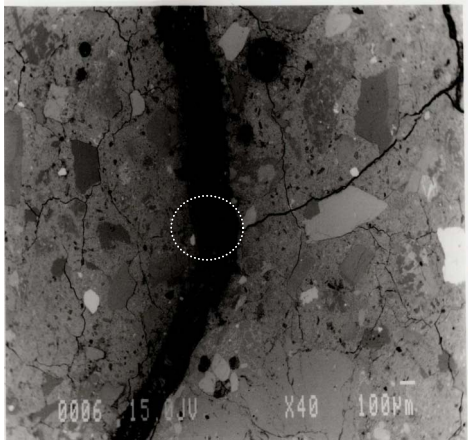
Crack widths and water-soluble chloride-ion concentrations for the cracked and uncracked regions of prism specimens are listed in **Table 11**. Here, crack widths measured after 15 years of exposure are also noted. Relatively lower chloride-ion concentrations were observed in uncracked regions. In the case of large crack widths, significant chloride-ion concentrations were observed in the cracked region. This is thought to be due to the accumulation of chloride ions near the crack, which is similar to the accumulation of chloride ions near the surface (**Fig. 7**). Where crack widths were small, slag cements showed the best performance against chloride ingress; chloride ingress for small crack widths (≤ 0.5 mm) was ordered as $\text{OPC} > \text{FACB} > \text{SCA} > \text{SCB} > \text{SCC}$, just as with uncracked concrete. However, the same ordering could not be confirmed for large (unhealed) crack widths, such as 1.5, 2, and 5 mm.

(4) Crack Healing (Prism Specimens)

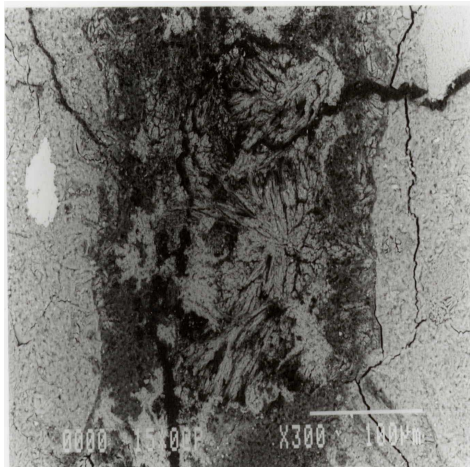
Small cracks (width ≤ 0.5 mm) were found to recover by autogenous healing irrespective of the types of cement. **Figure 11** shows one case of crack healing. A white deposit was observed in the crack plane, and the deposit also extended to the surface of the concrete. A detailed study of the process of autogenous healing in the laboratory concluded that the precipitation of calcium carbonate crystals (CaCO_3) in the cracks was almost its sole cause [19]. The water insoluble CaCO_3 evolves from a reaction between calcium ions derived from the concrete and bicarbonates or carbonates available in the water as shown below:



The pH of the seawater at the exposure location was around 7.8 (**Table 6**). The presence of alkalis in the crack region that had leached from the concrete and also alkalis produced by the reaction of sea salts and hydrated cement paste would increase the pH in a crack still further. Therefore, the reactions given above can be anticipated in the specimens investigated here.



— 100 μm



— 100 μm



— 10 μm

Fig.12 SEM micrographs of concrete surface cutting across the crack (SCB)

Table 12 Half-cell potential (vs Ag/AgCl)

Cover (cm)	Half-Cell Potential (mV)				
	OPC	SCA	SCB	SCC	FACB
2	-274	-367	-229	-413	-338
4	-229	-182	-182	-189	-120
7	-154	-176	-169	-189	-186

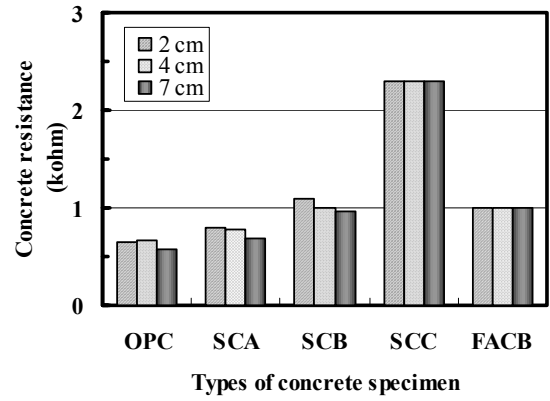


Fig. 13 Concrete resistance over the different cover depths

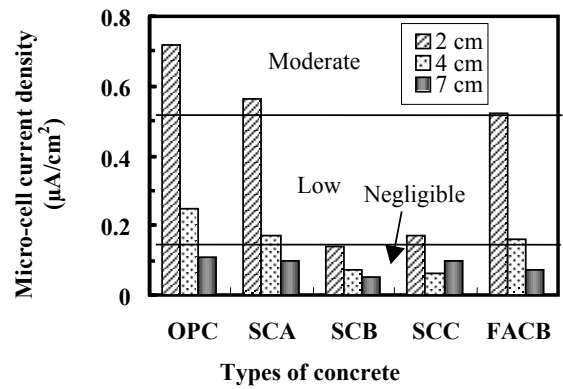


Fig. 14 Micro-cell current density at the different cover depths

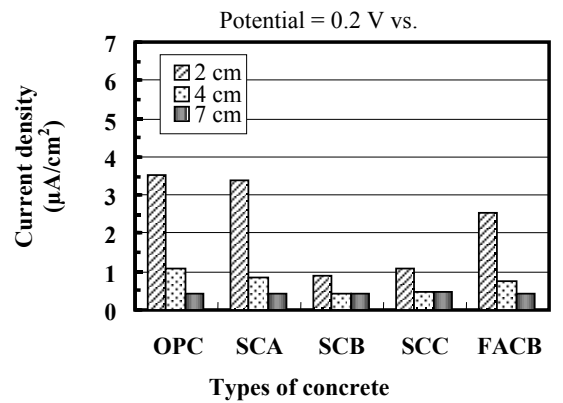


Fig. 15 Current density at anodic potential 0.2 V vs. SCE

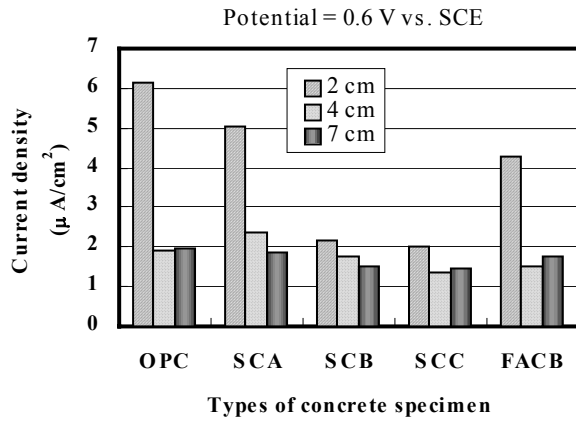


Fig. 16 Current density at anodic potential 0.6 V vs. SCE

The results of EPMA analysis indicated the presence of SO_3 with CaO and Al_2O_3 in the healed crack. This is evidence of the presence of ettringite ($3\text{CaO} \cdot \text{Al}_2\text{O}_3 \cdot 3\text{CaSO}_4 \cdot 32\text{H}_2\text{O}$) in the crack. EPMA results also indicated the presence of brucite ($\text{Mg}(\text{OH})_2$) in the healed crack. This is thought to arise as a result of reaction between magnesium salts in the seawater with cement hydration products. SEM micrographs at the cracked region are shown in **Fig. 12**. The needle-shaped ettringite is seen to be mixed with other deposits, such as calcite (CaCO_3) and brucite. Differences in healing progress with the various cement types could not be determined in this investigation. However, in Reference [19], based on a detailed laboratory study, it was concluded that the cement type has no influence on autogenous healing. Therefore, for a particular crack width, progress with healing can be assumed to be the same irrespective of cement type. Healed crack widths (≤ 0.5 mm) are defined here as small crack widths. Unhealed crack widths, such as 1.5 mm, 2 mm, and 5 mm, are defined as large crack widths.

(5) Corrosion of Steel Bars in Concrete: Electrochemical Evaluations

a) Uncracked Concrete (Cylinder Specimens)

The half cell potential data for all steel bars embedded in cylinder specimens are presented in **Table 12**. Where the cover depth was greater, a tendency toward lower negative potential was observed. In the case of SCC, a steel bar with 2 cm of cover showed a relatively more negative potential; however, the corroded area of the steel bar was lower compared with other cases. The data related to the corroded area are explained later. In another study [12], it was found that steel bars located at very high negative potentials do not corrode at all, even though the active corrosion potential was evaluated based on reference [7]. Therefore, based on this understanding of half cell potential, no order for the degree of corrosion of steel bars in different concretes is given here. Concrete resistance data over steel bars located at different cover depths are shown in **Fig. 13**. Generally, there is more ion movement in low-resistance concrete than in relatively high-resistance concrete. This leads to an increased corrosion rate in low-resistance concrete. Lower concrete resistance was observed in the case of OPC compared to slag and fly ash cements. SCC exhibited the highest resistance among the concretes (using different cements) investigated here. This means that the lowest corrosion activity can be expected for blended cements, especially for SCC and SCB compared to OPC. No significant difference in concrete resistance was observed for concrete where the cover depth was over 2, 4, and 7 cm. Making use of the polarization resistance data, the micro-cell current density of the steel bars was evaluated using the Stern-Geary equation, as follows [20]:

$$I_{mic} = \frac{B}{R_p} \times 10^6$$

$$B = \frac{\beta_a \beta_c}{2.3(\beta_a + \beta_c)}$$

Where, I_{mic} is the micro-cell current density in $\mu\text{A}/\text{cm}^2$, and the value of constant B depends on the anodic (β_a) and cathodic (β_c) polarization curve gradients. Assuming, β_a and β_c to be 120 mV/decade, the value of B can be estimated at 0.026 V [8], [20~21]. R_p is the polarization resistance in $\text{ohm} \cdot \text{cm}^2$. The calculated micro-cell current density values of steel bars located at different cover depths are shown in **Fig. 14**. The degree of corrosion, as based on these micro-cell current density values, was categorized as negligible, low, moderate, or high for current densities < 0.1 , $0.1-0.5$, $0.5-1.0$, and $> 1 \mu\text{A}/\text{cm}^2$, respectively [8]. Lower current densities were

Table 13 Passivity grades of the steel bars

Cover (cm)	Passivity Grades				
	OPC	SCA	SCB	SCC	FACB
2	3	3	4	3	3
4	3	4	4	4	3
7	4	4	4	4	4

observed where the cover depth was greater. This can be explained by the lower chloride-ion concentration as well as the lower oxygen permeability at greater cover depths [22~23]. At a cover depth of 2 cm, the current density was observed to be relatively higher in concrete made with OPC, FACB, and SCA. This is thought to be due to the presence of more chloride ions surrounding steel bars with 2 cm of cover (Fig. 7). There are also other factors, such as the ratio of Cl^-/OH^- and concrete resistance, that have a significant influence on corrosion rate [24~25]. Relatively less micro-cell corrosion was observed for concretes made with slag cements, especially SCC and SCB.

From the anodic polarization curves, current densities at potentials 0.2 V and 0.6 V were evaluated and the results are shown in Figs. 15 and 16. The current density was observed to be relatively lower in the case of slag cements, especially with SCC. Passivity grades of the steel bars as evaluated from the anodic polarization curves are listed in Table 13 based on reference [9]. A higher grades of passivity indicates less corrosion activity. A tendency toward higher passivity grade was observed for steel bars with more cover. Also, a tendency toward higher passivity grade was observed for steel bars in concretes made with slag cements. Based on the electrochemical results presented here, the degree of corrosion of steel bars in uncracked concrete can be ordered as $OPC > FACB > SCA > SCB > SCC$.

b) Cracked Concrete (Prism Specimens)

The micro-cell current density of a steel bar in the cracked region of a prism specimen is shown in Fig. 17. For small crack widths (≤ 0.5 mm), a tendency toward lower current density ($0.1-0.5 \mu A/cm^2$) was observed; this is a consequence of crack healing. It has already been mentioned that small cracks (width ≤ 0.5 mm) underwent healing during exposure in the tidal pool for 15 years. This healing caused the corrosion rate to fall or even reach zero. Where cracks had healed, no significant correlation between crack width (≤ 0.4 mm) and corrosion rate was found; however, a tendency for corrosion to be more rapid was observed for healed cracks measuring 0.5 mm (as compared to small cracks of width ≤ 0.4 mm). The physical evaluation yielded similar observations. The deposits were also found to cover the rust coating on the steel bar near the crack, as shown in Fig. 18. This can be expected to stop the corrosion process or significantly reduce the corrosion rate. The degree of corrosion can be ordered as $OPC > FACB > SCA > SCB > SCC$ for small crack widths.

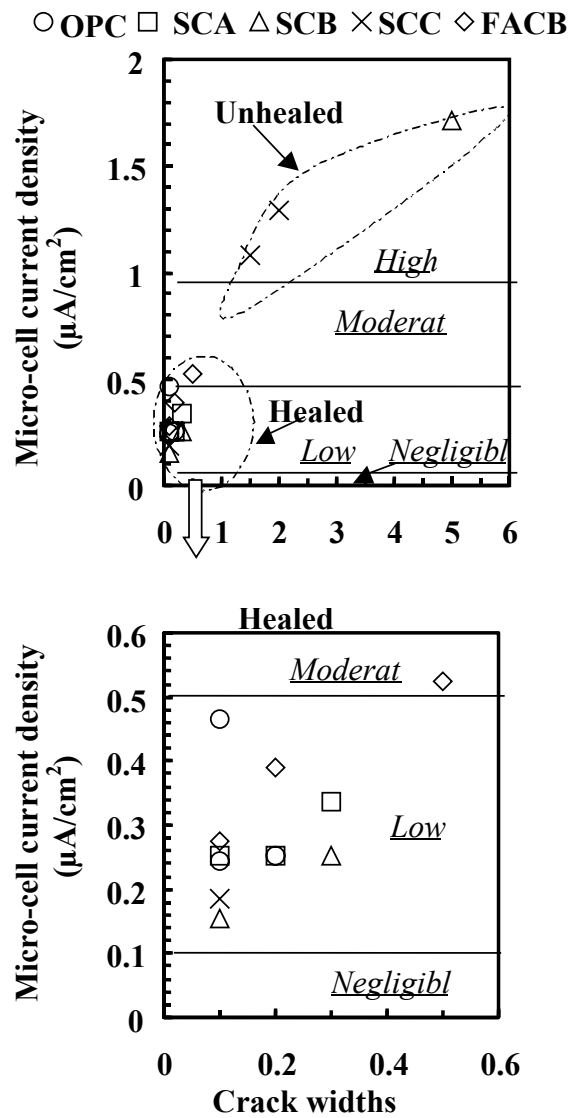


Fig. 17 Micro-cell current density at the cracked region (Top: Large and small crack widths, Bottom : Small crack widths)

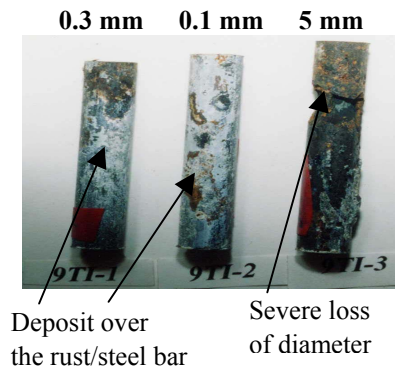


Fig. 18 Steel segments at the cracked region – SCB

Large crack widths (1.5, 2, and 5 mm) did not exhibit healing. Higher ($>1.0 \mu\text{A}/\text{cm}^2$) micro-cell current densities were observed in such cracks. Significant loss of steel bar diameter was observed, resulting from corrosion around the circumference of the bars as shown in **Fig. 18**. Corrosion induced by chloride ions is known to be an autocatalytic process. It reduces the pH around the steel bars leading to an accumulation of positive ions (Fe^{++}) in the cracked regions [26]. The excess positive charge is balanced by the migration of chloride ions. It is clear that in the case of small crack widths, the autocatalytic process comes to a halt or is reduced significantly as crack healing progresses. On the other hand, with larger cracks, the autocatalytic reaction continues and a significant loss of diameter results from corrosion of the steel bars. Very high concentrations of chloride ions were detected in the cracked region in the case of large crack widths (**Table 11**).

6) Corrosion of Steel Bars in Concrete: Physical Evaluations

a) Uncracked Concrete (Cylinder Specimens)

The corroded area of steel bars in uncracked specimens (cylinder specimens) is shown in **Table 14**. For a concrete cover of 2 cm, the corroded area was greatest in the case of FACB. Slag cements exhibited the best anti-corrosion performance. In the case of SCC, the corrosion was mostly concentrated where voids came into contact with the steel bar.

The number of pits and maximum pit depths are listed in **Table 15**. Steel bars in concretes made with OPC and FACB had more pitting than those in SCA, SCB, and SCC. Fewest pits were found on steel bars in SCC concrete. Based on these results, the degree of corrosion of steel bars in concrete can be ordered as $\text{OPC} > \text{FACB} > \text{SCA} > \text{SCB} > \text{SCC}$. This confirms the results obtained in the electrochemical evaluations described earlier.

Table 14 Corroded area of steel bars for the different cover depths – Cylindrical specimens

Cover (cm)	Corroded Area (cm^2) *				
	OPC	SCA	SCB	SCC	FACB
2	11.82	10.35	0.51	0	24.89
4	1.37	0	0	0	0
7	0	0	0	0	0

* Total area of bar = 51 cm^2 .

Table 15 Number of pits and maximum pit depth – Cylindrical specimens *

Cover (cm)	Number of Pits and Maximum Pit Depth (mm)				
	OPC	SCA	SCB	SCC	FACB
2	6 (1.5)	3 (1)	0 (0)	0 (0)	5 (0.5)
4	2 (1)	0 (0)	0 (0)	0 (0)	0 (0)
7	0 (0)	0 (0)	0 (0)	0 (0)	0 (0)

* Pit depths $<0.5 \text{ mm}$ are neglected. The figures in brackets represent the maximum pit depth in mm.

Table 16 Crack widths and maximum pit depths – Prism specimens

Specimen	Crack Width (mm) and Maximum Pit Depths in Cracked and Uncracked Regions (mm) *		
	1	2	3
OPC	0.2 (0.5) ((1.0))	0.1 (0) ((0.5))	0.1 (0.5) ((1.5))
SCA	0.1 (0) ((0))	0.3 (0.5) ((1.0))	0.2 (0) ((0))
SCB	0.3 (0.5) ((0))	0.1 (0) ((0))	5 (3.5**) ((0))
SCC	1.5 (1**) ((0))	0.1 (0) ((0))	2 (0.5**) ((0))
FACB	0.1 (0.5) ((0.5))	0.3 (1.0) ((0.5))	0.5 (1.5) ((0.5))

*The figures in (.) and ((.)) represent maximum pit depths in cracked and uncracked regions, respectively. Pit depths $< 0.5 \text{ mm}$ are not counted. The figures without bracket represent crack widths. Unhealed cracks are shown in bold-italic type. **Significant loss of diameter observed due to corrosion around the circumference of steel bars.

Table 17 Crack width and total number of pits – Prism specimens

Specimen	Crack Widths (mm) and Pit Count		
	1	2	3
OPC	(0.2) 7	(0.1) 5	(0.1) 8
SCA	(0.1) 0	(0.3) 7	(0.2) 7
SCB	(0.3) 2	(0.1) 0	(5) 3
SCC	(1.5) 1	(0.1) 0	(2) 1
FACB	(0.1) 4	(0.3) 4	(0.5) 4

The figures in (.) represent crack widths in mm.

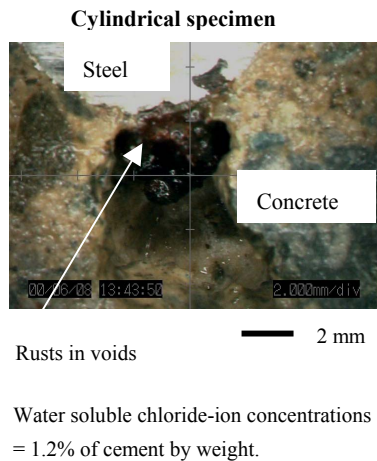


Fig.19 Steel-concrete interface of cylindrical specimen – SCB

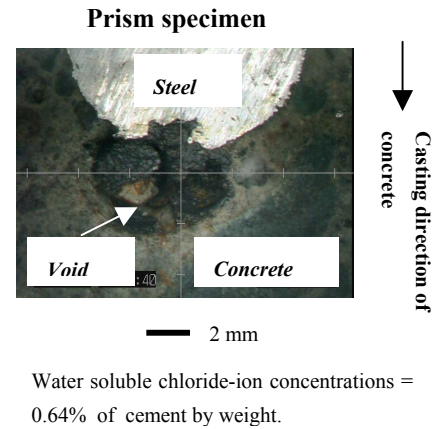


Fig.20 Pit on the steel bar due to void (Prism Specimen – OPC)

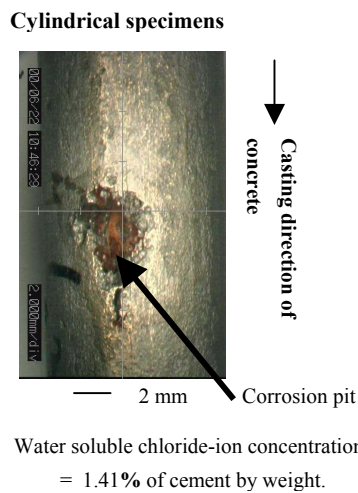


Fig.21 Pit on the steel bar due to void (Prism Specimen – SCA)

b) Cracked Concrete (Prism Specimens)

The maximum depth of pits on steel bars in the cracked and uncracked regions of prism specimens are listed in **Table 16**. For small cracks (width ≤ 0.5 mm), the maximum depth did not necessarily occur in the cracked region. This can be explained by the crack healing described earlier. Bars embedded in SCC concrete exhibited the least number of pits. Total pit numbers are listed in **Table 17** for all concretes. Pit numbers were lower in the case of all slag cements, with SCC the lowest as already noted. For small cracks, the degree of steel bar corrosion can be ordered as OPC>FACB>SCA>SCB>SCC, which is the same result as for uncracked concrete. This also acts as confirmation of the electrochemical results given before. For large cracks (of width 1.5, 2, and 5 mm), significant loss of diameter was found to have resulted from corrosion around the circumference of the steel bars (**Fig. 18** and **Table 16**). Unfortunately, due to the limited number of data points recorded for large cracks, the performance of the cements investigated here cannot be compared. Further investigations will be necessary in this area. Based on the limited data available, deep, localized corrosion is suspected in the case of blended cements (**Table 16**). It is inferred that, in order to enhance the durability of concrete structures in marine environments, crack widths should be restricted as much as possible to allow for possible healing during exposure.

(7) Influence of Voids at Steel-Concrete Interface

Several detailed laboratory and long-term exposure investigations on the influence of voids at the steel-concrete interfaces have been reported [27~30]. Here, voids are defined as those that are visible to the naked eye. The size

of such voids is of the order of a millimeter to a few millimeters in diameter. From this study, it was observed that the presence of voids at the steel-concrete interface resulted in the formation of corrosion pits. Where the steel-concrete interface was sound, there was no steel bar corrosion even with a chloride-ion concentration much greater than the chloride threshold limit (defined as 0.4% of cement by weight). Microscopic observations of corrosion pit formation as a result of voids at the steel-concrete interface are shown in **Figs. 19–21**. If the casting direction of the concrete is perpendicular to the steel bar (**Fig. 20**, Prism specimens), voids tend to form under the steel bars due to settlement of the concrete under gravity as well as by the trapping of bleed water under the bar. Voids may also form surrounding the steel bar, even though the casting direction is along the axis of the steel bar (**Fig. 19**, Cylinder Specimens), due to poor concrete compaction. During this investigation, it was observed that in the case of slag cements there was little corroded area, and the corrosion that did occur was concentrated around voids at the steel-concrete interface. Therefore, in order to enhance the long-term durability of concrete structures in a marine environment, it is important to keep the steel-concrete interface free of voids

(8) Remaining Studies

Studies of concrete microstructure (porosity), surface morphology (SEM), and chemical composition (XRD and EPMA) for concretes made with the cements investigated here are still ongoing. Further results will be reported in future. Some of the specimens have been retained at the exposure site, and will be studied after 20 years of exposure.

5. CONCLUSIONS

Based on investigations of 15-year-old uncracked and precracked concrete specimens made with W/C=0.45 and different kinds of cement, consisting of ordinary Portland cement (OPC), slag cements of type A (SCA), B (SCB), and C (SCC), and fly ash cement of type B (FACB), the following conclusions have been drawn:

1. Chloride ingress and steel bar corrosion can be ordered as OPC>FACB>SCA>SCB>SCC in terms of severity for uncracked and cracked concrete with small cracks (width ≤ 0.5 mm).
2. After 15 years of exposure in a tidal environment, the compressive strength of all concretes except FACB meets the corresponding 28-day design strength.
3. Small cracks (width ≤ 0.5 mm) undergo healing irrespective of cement type.
4. The presence of visible voids at the steel-concrete interface causes the formation of corrosion pits irrespective of cement type.
5. In order to enhance the long-term durability of concrete structures, crack widths should be controlled to allow for possible healing during exposure, and care should be taken to ensure that there are no voids at the steel-concrete interface.

ACKNOWLEDGEMENTS: The authors wish to express their gratitude and sincere appreciation to the authorities at the *Port and Airport Research Institute, Independent Administrative Institution, Yokosuka, Japan* for their support in performing this investigation. Thanks are also due to members of the *Materials Division* of the *Port and Airport Research Institute* for their kind help during the experimental work. Finally, thanks are due to earlier members of the *Materials Division* of the *Port and Airport Research Institute* for initiating the exposure of these valuable specimens 15 years ago.

References

- [1] Nagataki, S., “Mineral Admixtures in Concrete: State of the Art and Trends”, Proceedings of V. Mohan Malhotra on Concrete Technology Past, Present and Future, *ACI SP 144*, pp. 447-482, 1993.
- [2] Mehta, P. K., “Pozzolanic and Cementitious By-products as Mineral Admixtures for Concrete – A Critical Review”, Proc. Of the CANMET/ACI First International Conference, *ACI SP 79*, Vol. 1, pp. 1-46, 1983.
- [3] Malhotra, V.M., “Fly Ash, Slag, Silica Fume, and Rice-Husk Ash in Concrete : A Review”, *ACI Concrete International*, Volume 15, No. 4, pp. 23-28, 1993.
- [4] RILEM Report, “Fly Ash in Concrete – Properties and Performance”, Editor: Wesche, K., Chapman and Hall, 1991.
- [5] Malhotra, V.M. and Mehta, P.K., “Pozzolanic and Cementitious Materials, Advances in Concrete Technology”, Vol. 1, Gordon and Breach Publishers, Canada, 1996.

- [6] Standard Specification for Design and Construction of Concrete Structures, Japan Society of Civil Engineers, Part 2 (Construction), SP-2, First Edition, 1986.
- [7] ASTM C876-91, Standard Test Methods for Half-Cell Potential of Uncoated Reinforcing Steel in Concrete, 1991.
- [8] Andrade, C. and Alonso, C., “On-site Measurement of Corrosion Rate of Reinforcements”, Fifth CANMET/ACI International Conference on Durability of Concrete, Barcelona, Spain 2000, Proceedings of a Special Technical Session on “Near-Surface Testing for Strength and Durability of Concrete”, Ed. Basheer, P.A.M., pp.171-183, 2000.
- [9] Otsuki, N., Nagataki, S., and Nakashita, K., “Evaluation of AgNO₃ Solution Spray Method for Measurement of Chloride Penetration into Hardened Cementitious Materials”, *ACI Materials Journal*, Vol. 89, No. 6, pp. 587-592, Nov.-Dec. 1992.
- [10] Brown, R.D., “Mechanism of Corrosion of Steel in Concrete in Relation to Design, Inspection and Repair of Offshore and Coastal Structures, Performance of Concrete in Marine Environment”, *ACI SP 65*, pp. 169-204, 1980.
- [11] Fukute, T. and Hamada, H., “A Study on the Durability of Concrete Exposed in Marine Environment for 20 Years”, *Report of the Port and Harbour Research Institute*, Ministry of Transport, Japan, Vol. 31, No. 5, pp. 251-272, March 1993.
- [12] Mohammed, T.U., Otsuki, N., Hisada, M., and Hamada, H., “Marine Durability of 23-Year-Old Reinforced Concrete Beams”, Fifth CANMET/ACI International Conference on Durability of Concrete, Barcelona, Spain, *ACI SP 192-65*, pp.1071-1088, 2000.
- [13] Sakai, K., “Long-Term Performance of Concrete in a Marine Environment”, Third CANMET/ACI International Conference on Performance of Concrete in Marine Environment, pp. 35-53, August 1996.
- [14] Sakai, K. and Sasaki, S., “Ten-Year Exposure Test of Pre-Cracked Reinforced Concrete Specimens in a Marine Environment”, *ACI SP145-18*, pp. 353-369, 1994.
- [15] Hansen, E. J. and Saouma, V.E., “Numerical Simulation of Reinforced Concrete Deterioration – Part I: Chloride Diffusion”, *ACI Materials Journal*, Vol. 96, No. 2, pp. 173-180, March-April 1999.
- [16] Rasheeduzzafar, A.S., Dakhil, S.S., and Al-Gahtani, A.S., “Effect of Cement Composition on Corrosion of Reinforcing Steel in Concrete”, Third International Symposium on Corrosion of Reinforcement in Concrete Construction, U.K., Edited by Page, C.L., pp. 213-226, 1990.
- [17] Mehta, P.K., “Durability of Concrete Exposed to Marine Environment – A Fresh Look”, 2nd CANMET/ACI International Conference on Durability of Concrete, Canada, *ACI SP 109-1*, pp. 1-29, 1991.
- [18] Rosenberg, A., Grace, W.R. and Hansson, M.C., “Mechanisms of Corrosion of Steel in Concrete”, *Materials Science of Concrete*, Vol. 1, Skanly Jp. Ed., MRS, pp. 285-316, 1989.
- [19] Edvardsen, C., “Water Permeability and Autogenous Healing of Cracks in Concrete”, *ACI Materials Journal*, V. 96, No. 4, pp. 448-454, July – August 1999.
- [20] Fontana, M. G. and Greene, N. D., “Corrosion Engineering”, Second Edition, McGraw-Hill, 1983.
- [21] Gu, P., Beaudoin, J.J., Zhang, M.H., and Malhotra, V.M., “Performance of Reinforcing Steel in Concrete Containing Silica Fume and Blast-Furnace Slag Ponded with Sodium Chloride Solution”, *ACI Materials Journal*, Vol. 97, No. 3, pp. 254-262, May-June 2000.
- [22] GjØrv, O.E., Vennesland, O., and El-Busaidy, A.H.S., “Diffusion of Dissolved Oxygen Through Concrete”, *Materials Performance*, 25, 12, pp. 38-44, 1986.
- [23] Sandberg, P., “Cost Effective Service Life Design of Concrete Structures in Saline Environment”, Proceedings of the International Conference on Durability of Building Materials and Components, Vol. 2, pp. 1195-1214, 1996.
- [24] Mehta, P.K., “Concrete: Structure, Properties and Materials”, Prentice-Hall, Englewood Cliffs, New Jersey.
- [25] Monterio, P.J.M., GjØrv, O.E., and Mehta, P.K., “Microstructure of the Steel-Cement Paste Interface in the Presence of Chloride”, *Cement and Concrete Research*, Vol. 15, pp. 781-784, 1985.
- [26] Gu, P., Beaudoin, J.J., Tumidajski, P.J., and Mailvaganam, N.P., “Electrochemical Incompatibility of Patches in Reinforced Concrete”, *Concrete International*, Vol. 19, No. 8, pp. 68-72, August 1997.
- [27] Mohammed, T.U., Otsuki, N., and Hisada, M., “Corrosion of Steel Bars with Respect to Orientation in Concrete”, *ACI Material Journal*, Vol. 96, No. 2, pp. 154-159, March-April 1999.
- [28] Mohammed, T.U., Hamada, H., Otsuki, N., and Toru, Y., “Chloride-ion Induced Corrosion of Steel Bars in Concrete with the Presence of Gap at the Steel-Concrete Interface”, *ACI Materials Journal*, Vol. 99, No. 2, pp. 149-156, March-April 2002.
- [29] Mohammed, T.U., Otsuki, N., Hamada, H., and Watanabe, H., “Several Issues in Designing Durable RC Structures”, *Journal of JCI*, Vol. 38, No. 11, pp. 36-41, November 2000 (Japanese).
- [30] Mohammed, T.U., “A Study on Corrosion of Plain and Deformed Steel Bars With Respect to Bar Orientation and Cracks in Concrete”, Doctoral Thesis, Department of Civil Engineering, Tokyo Institute of Technology, Japan, September 1997.